PHYSICAL REVIEW B VOLUME 31, NUMBER 12 15 JUNE 1985

Intensities and asymmetries of electronic Raman scattering in $ErPO_4$ and $TmPO_4$

P. C. Becker, N. Edelstein, G. M. Williams, J. J. Bucher, and R. E. Russo
Materials and Molecular Research Division, Lawrence Berkeley Laboratory, Berkeley, California 94720 and Department of Physics, University of California, Berkeley, California 94720

J. A. Koningstein
Department of Chemistry, Carleton University, Ottawa, Ontario, Canada

L. A. Boatner and M. M. Abraham
Solid State Division, Oak Ridge National Laboratory, Oak Ridge, Tennessee 37830
(Received 28 January 1985)

An investigation of the low-temperature electronic Raman scattering spectra of $ErPO_4$ and $TmPO_4$ has been carried out. The experimental intensities have been compared with the standard second-order theory of two-photon processes for both intermultiplet and intramultiplet transitions between individual crystal-field levels. Adequate agreement is found in the case of $ErPO_4$, but serious discrepancies exist for $TmPO_4$. It is shown that electronic Raman scattering is a sensitive technique for testing the Judd-Ofelt—type theories of two-photon processes in rare-earth crystals. Strong asymmetry, a characteristic feature of electronic Raman scattering, has been observed in several of the transitions.

I. INTRODUCTION

Nonlinear laser spectroscopy has proven to be a fruitful area of research in investigating the optical behavior of rare-earth ions in crystalline hosts.[1–5] In particular, two-photon absorption by $4f^7$ systems in LaF_3 has recently been extensively studied, and has led to a reformulation and extension of the second-order theory of Axe for two-photon processes[6] by the inclusion of higher-order terms in the perturbation expansion.[2–5] Electronic Raman scattering is a two-photon process and is formally equivalent to two-photon absorption.[6–10] Comparison of the experimental and calculated intensities of the electronic Raman transitions in rare-earth-doped crystals is another test of the adequacy of the theory. In addition, electronic Raman spectra display asymmetric features[11] (e.g., $I_{XZ} \neq I_{ZX}$, where the subscripts indicate the respective polarizations of the incident and scattered photons) which are a very sensitive test of the second-order theory. This asymmetry cannot be observed in two-photon absorption experiments that use only one input beam.

The room-temperature Raman spectra of $ErPO_4$ and $TmPO_4$ have been reported,[12] as well as the low-temperature Raman spectrum of $TmPO_4$.[13] The energy levels of Er^{3+} and Tm^{3+} in phosphate hosts are well known and crystal-field analyses have been performed[14,15] for the rare-earth ion at a D_{2d}-symmetry site. Accurate wave functions are thus available for quantitative calculations of the electronic Raman intensities according to the second-order theory. We present and analyze here detailed experimental data on the electronic Raman scattering spectra of the crystals $TmPO_4$ and $ErPO_4$. Implicit in this treatment is the assumption that we can use a single-ion theory for the pure crystal.

II. EXPERIMENTAL

The Raman scattering was excited with a cw argon-ion laser in a 90° geometry, operated at 50—100 mW. For $ErPO_4$ we used the lines at 514.5 and 457.9 nm, and for $TmPO_4$ the lines at 514.5 and 488.0 nm, since these lines do not overlap any absorption features. Taking into account the ω^4 dependence (ω being the frequency of the scattered photon) and the detection system's spectral characteristics, the relative intensities were found to be independent of the excitation wavelength.

The samples used were usually in the form of plates, with typical dimensions 1 mm × 5 mm × 15 mm. Their chemical and structural properties have been described elsewhere.[16–19(a)] A Janis Supertran cold-finger Dewar was used for the low-temperature experiments. The temperature was measured with a silicon-diode temperature sensor, at a copper block to which the sample was attached. The sample temperature was estimated to be in the range of 5 to 15 K (approximately 10 K) when the Dewar was operated with liquid helium and the temperature sensor read 4.2 K. At 77 K and above, it appears that the sample temperature is the same as that of the sensor, as determined from Stokes—anti-Stokes measurements. Spectra were taken at 295, 77, and approximately 10 K. At 295 K, only the phonon spectrum was found. The sample had to be cooled below 80 K before the electronic lines were detectable since they exhibited strong temperature broadening as the temperature increased. All intensity measurements were made at approximately 10 K. At that temperature, all the observed electronic Raman transitions originate in the ground state. The scattered light was analyzed with a SPEX 1403 double monochromator followed by photon-counting detection. The spectral bandpass was approximately 2 cm^{-1}.

For each scan, the polarization characteristics of the phonon lines were checked to ensure that the crystal was properly aligned, and the intensity measurements were retained only for those scans for which the phonon selection rules were obeyed. In particular, the Raman tensor of the E_g (Γ_5) phonon lines were checked for symmetry (e.g., $I_{XZ}=I_{ZX}$) since the measurement of the asymmetry of the electronic lines is one of the major motivations for this work. As noted previously,[20] the most significant polarization leakage is between the Γ_3 and Γ_4 symmetries. This does not affect the asymmetry measurements, which are contained in lines of Γ_5 symmetry. The electronic Raman intensities were averaged over several samples, crystal orientations, and excitation wavelengths to improve their accuracy. The maximum relative error on these intensities is about 25%.

III. SYMMETRY AND SELECTION RULES

$ErPO_4$ and $TmPO_4$ have the tetragonal zircon structure (space group D_{4h}^{19}). There are four rare-earth ions per unit cell, located at sites of D_{2d}-point-group symmetry. A primitive cell containing only two rare-earth ions can also be defined.[19(b)] The vibrational spectrum can be assigned by means of the factor group D_{4h} (the symmetry group of the unit cell). Note, however, that the two C_2 axes of the D_{2d}-symmetry rare-earth site are rotated about the Z axis by 45° relative to the X and Y axes (X,Y,Z refer to the axes of the unit cell). Hence care must be taken in the construction of the electronic Raman scattering matrices. Tensors calculated in terms of the D_{2d} local symmetry rare-earth site need to be rotated by 45° when expressed in terms of the X,Y,Z crystallographic axes. The 45° rotation interchanges the Γ_3 and Γ_4 symmetries. Neglect of this rotation led to the incorrect identification of the Γ_3 (B_1) line at 84 cm^{-1} as being of symmetry Γ_4 (B_2) in $TmPO_4$.[13]

Tm^{3+} is an f^{12} system for which the states are classified according to the irreducible representations Γ_1 through Γ_5 of D_{2d}. Er^{3+} is an f^{11} system characterized by the double representations Γ_6 and Γ_7. The electronic scattering tensors, both symmetric and antisymmetric, that correspond to the various irreducible representations are as follows:[21]

$$\alpha_{xx}+\alpha_{yy},\ \alpha_{zz} \quad \text{for } \Gamma_1 ,$$
$$\alpha_{xy}-\alpha_{yx} \quad \text{for } \Gamma_2 ,$$
$$\alpha_{xx}-\alpha_{yy} \quad \text{for } \Gamma_3 ,$$
$$\alpha_{xy}+\alpha_{yx} \quad \text{for } \Gamma_4 ,$$
$$\alpha_{xz}\pm\alpha_{zy},\ \alpha_{yz}\pm\alpha_{zy} \quad \text{for } \Gamma_5 .$$

The scattering tensors that correspond to the transitions can then be obtained via the direct product of the initial- and final-state representations. For Tm^{3+} the ground state is Γ_1, therefore the symmetry of the transition is the symmetry of the final state. For Er^{3+} the ground state is Γ_7 and we have, for the transition $\Gamma_7\rightarrow\Gamma_7$, the scattering tensor $\Gamma_1+\Gamma_2+\Gamma_5$ and for $\Gamma_7\rightarrow\Gamma_6$ the scattering tensor $\Gamma_3+\Gamma_4+\Gamma_5$. It should be noted that the presence of antisymmetric tensors in several of these transitions is one of the central features of electronic Raman scattering. The relationship between the scattering matrix of the crystal and the scattering tensors at the sites is discussed in the following section.

IV. THEORETICAL ANALYSIS

The wave functions of the rare-earth-ion-crystal-field levels can be written in terms of Russell-Saunders coupled wave functions:

$$\Psi_n=\sum_{S,L,J,J_z} a(n;\gamma,S,L,J,J_z)\,|\,\gamma,S,L,J,J_z\rangle \ . \tag{1}$$

Using the second-order theory, Koningstein and Mortensen derived the following expression for the Raman tensor for a transition from state k to state n:[7,9,22]

$$(\alpha_Q^K)_{kn}=F(K,\nu)\sum_{\gamma,S,L,J,J_z}\ \sum_{\gamma',S,L',J',J_z'} a^*(n;\gamma',S,L',J',J_z')\,a(k;\gamma,S,L,J,J_z)\langle\gamma',S,L',J',J_z'\,|\,U_Q^K\,|\,\gamma,S,L,J,J_z\rangle \ , \tag{2}$$

where $K=1,2$; U_Q^K is the unit tensor, and

$$F(K,\nu)=\frac{1}{h}\sum_{\chi}\left[\frac{1}{\bar{\nu}_{\chi k}-\nu}+(-1)^K\frac{1}{\bar{\nu}_{\chi k}+\nu}\right](l||c^{(1)}||l')^2\langle nl||r||n'l'\rangle^2(2K+1)^{1/2}\begin{Bmatrix}1 & K & 1\\ l & l' & l\end{Bmatrix}(-1)^K . \tag{3}$$

$h\bar{\nu}_{\chi k}$ is the center of gravity of the intermediate-excited-state configuration χ, ν is the frequency of the exciting line, and l and l' are the respective orbital quantum numbers of the ground-state level and the excited-state level. In our calculations we have retained $\chi=(4f)^{n-1}5d$, the ground state having the configuration $(4f)^n$, so that $l=3$ and $l'=2$. The unit tensor matrix elements are easily evaluated.[23,24] The α_Q^K are then transformed[8] into the α_{ij} ($i,j=X,Y,Z$).[25]

The elements of the scattering matrix are obtained from the elements of the scattering tensors of the individual ions at the two sites in the primitive cell. Since the local axes of these two sites are related to each other by an inversion center their scattering tensors are identical. This scattering tensor is rotated by 45° so that the scattering matrix can be expressed in the crystallographic X,Y,Z axes. Note that for Er^{3+} each level is a Kramers doublet. The elements of the scattering tensor are evaluated between individual Kramers levels, squared, and then summed to obtain the scattering matrix for the transition

TABLE I. Crystal-field energy levels and wave functions for Er^{3+} (energies in cm^{-1}).

Energy[a]	Energy[b]	Symmetry	Wave function $^{2S+1}L \mid J,J_z\rangle$[c]
0	0	Γ_7	$-0.8446\,^4I \mid \frac{15}{2},\frac{7}{2}\rangle - 0.3060\,^4I \mid \frac{15}{2},-\frac{1}{2}\rangle$ $-0.2922\,^4I \mid \frac{15}{2},\frac{15}{2}\rangle - 0.2787\,^4I \mid \frac{15}{2},-\frac{9}{2}\rangle$
36	33	Γ_6	$+0.8258\,^4I \mid \frac{15}{2},\frac{5}{2}\rangle + 0.4765\,^4I \mid \frac{15}{2},-\frac{3}{2}\rangle$ $+0.1849\,^4I \mid \frac{15}{2},-\frac{11}{2}\rangle + 0.2787\,^4I \mid \frac{15}{2},\frac{13}{2}\rangle$
53	53	Γ_7	$-0.8877\,^4I \mid \frac{15}{2},-\frac{9}{2}\rangle + 0.2915\,^4I \mid \frac{15}{2},\frac{7}{2}\rangle$ $+0.2273\,^4I \mid \frac{15}{2},\frac{15}{2}\rangle - 0.2129\,^4I \mid \frac{15}{2},-\frac{1}{2}\rangle$
98	105	Γ_7	$-0.9114\,^4I \mid \frac{15}{2},\frac{15}{2}\rangle + 0.3298\,^4I \mid \frac{15}{2},\frac{7}{2}\rangle$ $-0.0942\,^4I \mid \frac{15}{2},-\frac{1}{2}\rangle + 0.1476\,^4I \mid \frac{15}{2},-\frac{9}{2}\rangle$
132[d]	145	Γ_6	$-0.6757\,^4I \mid \frac{15}{2},-\frac{11}{2}\rangle - 0.5474\,^4I \mid \frac{15}{2},-\frac{3}{2}\rangle$ $+0.4384\,^4I \mid \frac{15}{2},\frac{5}{2}\rangle + 0.1464\,^4I \mid \frac{15}{2},\frac{13}{2}\rangle$
229[d]		Γ_6	$-0.6884\,^4I \mid \frac{15}{2},-\frac{11}{2}\rangle + 0.6511\,^4I \mid \frac{15}{2},-\frac{3}{2}\rangle$ $-0.1957\,^4I \mid \frac{15}{2},\frac{13}{2}\rangle - 0.1831\,^4I \mid \frac{15}{2},\frac{5}{2}\rangle$
246[d]		Γ_7	$-0.9066\,^4I \mid \frac{15}{2},-\frac{1}{2}\rangle + 0.2871\,^4I \mid \frac{15}{2},-\frac{9}{2}\rangle$ $+0.2510\,^4I \mid \frac{15}{2},\frac{7}{2}\rangle$
286[d]		Γ_6	$+0.9397\,^4I \mid \frac{15}{2},\frac{13}{2}\rangle - 0.2496\,^4I \mid \frac{15}{2},\frac{5}{2}\rangle$ $+0.1382\,^4I \mid \frac{15}{2},-\frac{3}{2}\rangle$

[a]Observed energy levels for Er^{3+}:$LuPO_4$.
[b]Observed energy levels for $ErPO_4$ from the electronic Raman spectra.
[c]Wave functions for Er^{3+}:$LuPO_4$, from the crystal-field fit.
[d]Not observed, obtained from the crystal-field fit.

between the Kramers doublets.

For $ErPO_4$ and $TmPO_4$, crystal-field fits based on optical-absorption experiments have been reported so that the coefficients $a(n;\gamma,S,L,J,J_z)$ are available.[14,15] Tables I and II list the wave functions for Er^{3+}:$LuPO_4$ and Tm^{3+}:$LuPO_4$, respectively. Only those multiplets involved in observed transitions are listed. The wave functions for Er^{3+}:YPO_4 (Ref. 14) and Tm^{3+}:YPO_4 (Ref. 15) were also tested and were found to yield almost identical relative intensities as the above wave functions. The only differences were in the case of Tm^{3+} for the 303-cm^{-1} transition (eight times larger with YPO_4 wave functions) and the 321-cm^{-1} transition (five times smaller with YPO_4 wave functions). We have assumed that the Er^{3+}:$LuPO_4$ and Tm^{3+}:$LuPO_4$ wave functions are representative of the pure crystals $ErPO_4$ and $TmPO_4$.

It can be seen from Eq. (3) that a comparison of the relative intensities of the electronic Raman transitions involves only one adjustable parameter, namely, the ratio $F(1,\nu)/F(2,\nu)$. If only the $(4f)^{n-1}5d$ configuration is used for the intermediate levels, and assuming $\nu \ll \bar{\nu}_{\chi k}$, this ratio is given by the simple relation

TABLE II. Crystal-field energy levels and wave functions for Tm^{3+} (energies in cm^{-1}).

Energy[a]	Energy[b]	Symmetry	Wave function $^{2S+1}L \mid J,J_z\rangle$[c]
0	0	Γ_1	$+0.8455\,^3H \mid 6,0\rangle + 0.3713\,^3H \mid 6,-4\rangle + 0.3713\,^3H \mid 6,4\rangle$
25	30	Γ_5	$+0.7386\,^3H \mid 6,-1\rangle + 0.5868\,^3H \mid 6,-5\rangle + 0.3175\,^3H \mid 6,3\rangle$
80	86	Γ_3	$+0.6950\,^3H \mid 6,-2\rangle + 0.6950\,^3H \mid 6,2\rangle$ $+0.1128\,^3H \mid 6,-6\rangle + 0.1128\,^3H \mid 6,6\rangle$

TABLE II. (*Continued*).

Energy[a]	Energy[b]	Symmetry	Wave function $^{2S+1}L \mid J,J_z\rangle$[c]
125	138	Γ_5	$+0.7903\,^3H \mid 6,-5\rangle - 0.4573\,^3H \mid 6,-1\rangle - 0.3972\,^3H \mid 6,3\rangle$
183[d]		Γ_2	$-0.7040\,^3H \mid 6,4\rangle + 0.7040\,^3H \mid 6,-4\rangle$
248[d]		Γ_1	$+0.5978\,^3H \mid 6,-4\rangle + 0.5978\,^3H \mid 6,4\rangle - 0.5257\,^3H \mid 6,0\rangle$
254[d]		Γ_4	$-0.5648\,^3H \mid 6,2\rangle + 0.5647\,^3H \mid 6,-2\rangle$ $+0.4203\,^3H \mid 6,-6\rangle - 0.4203\,^3H \mid 6,6\rangle$
281[d]	280	Γ_5	$-0.8559\,^3H \mid 6,3\rangle + 0.4862\,^3H \mid 6,-1\rangle - 0.1487\,^3H \mid 6,-5\rangle$
303[d]		Γ_3	$-0.6949\,^3H \mid 6,-6\rangle - 0.6948\,^3H \mid 6,6\rangle$ $+0.1131\,^3H \mid 6,-2\rangle + 0.1131\,^3H \mid 6,2\rangle$
321[d]		Γ_4	$+0.5648\,^3H \mid 6,6\rangle - 0.5646\,^3H \mid 6,-6\rangle$ $-0.4202\,^3H \mid 6,2\rangle + 0.4202\,^3H \mid 6,-2\rangle$
5587[d]	5602	Γ_3	$-0.5561\,^3F \mid 4,2\rangle - 0.5561\,^3F \mid 4,-2\rangle$ $+0.2043\,^3H \mid 4,2\rangle + 0.2043\,^3H \mid 4,-2\rangle$ $-0.3857\,^1G \mid 4,2\rangle - 0.3857\,^1G \mid 4,-2\rangle$
5674	5688	Γ_5	$-0.6014\,^3F \mid 4,-1\rangle - 0.5167\,^3F \mid 4,3\rangle$ $+0.2164\,^3H \mid 4,-1\rangle + 0.1817\,^3H \mid 4,3\rangle$ $-0.4097\,^1G \mid 4,-1\rangle - 0.3486\,^1G \mid 4,3\rangle$
5700[d]	5676	Γ_1	$-0.4998\,^3F \mid 4,4\rangle - 0.4998\,^3F \mid 4,-4\rangle - 0.3648\,^3F \mid 4,0\rangle$ $+0.1747\,^3H \mid 4,4\rangle + 0.1747\,^3H \mid 4,-4\rangle + 0.1300\,^3H \mid 4,0\rangle$ $-0.3371\,^1G \mid 4,4\rangle - 0.3371\,^1G \mid 4,-4\rangle - 0.2477\,^1G \mid 4,0\rangle$
5735[d]		Γ_2	$-0.5642\,^3F \mid 4,-4\rangle + 0.5641\,^3F \mid 4,4\rangle$ $+0.1951\,^3H \mid 4,-4\rangle - 0.1951\,^3H \mid 4,4\rangle$ $-0.3785\,^1G \mid 4,-4\rangle + 0.3785\,^1G \mid 4,4\rangle$
5763		Γ_4	$-0.5620\,^3F \mid 4,-2\rangle + 0.5620\,^3F \mid 4,2\rangle$ $+0.1971\,^3H \mid 4,-2\rangle - 0.1971\,^3H \mid 4,2\rangle$ $-0.3800\,^1G \mid 4,-2\rangle + 0.3800\,^1G \mid 4,2\rangle$
5842		Γ_5	$-0.6106\,^3F \mid 4,3\rangle + 0.5190\,^3F \mid 4,-1\rangle$ $+0.2048\,^3H \mid 4,3\rangle - 0.1783\,^3H \mid 4,-1\rangle$ $-0.4025\,^1G \mid 4,3\rangle + 0.3462\,^1G \mid 4,-1\rangle$
5857[d]	5870	Γ_1	$+0.7113\,^3F \mid 4,0\rangle - 0.2614\,^3F \mid 4,4\rangle - 0.2614\,^3F \mid 4,-4\rangle$ $-0.2410\,^3H \mid 4,0\rangle$ $-0.1722\,^1G \mid 4,4\rangle - 0.1722\,^1G \mid 4,-4\rangle + 0.4714\,^1G \mid 4,0\rangle$

[a]Observed energy levels for Tm^{3+}:$LuPO_4$.
[b]Observed energy levels for $TmPO_4$ from the electronic Raman spectra.
[c]Wave functions for Tm^{3+}:$LuPO_4$, from the crystal-field fit.
[d]Not observed, obtained from the crystal-field fit.

TABLE III. Frequencies (cm^{-1}) and symmetries of the Raman-active phonons of $ErPO_4$ and $TmPO_4$ at 295, 77, and approximately 10 K.

	E_g	B_{1g}	E_g	B_{1g}	E_g	B_{2g}	A_{1g}	E_g	B_{1g}	B_{1g}	E_g	A_{1g}
							(a) $ErPO_4$					
295 K	132	a	185	b	299	330	486	578	658	1003	1023	1060
77 K	132	140	185	b	302	330	488	580	659	1004	1026	1063
10 K	133	140	186	b	303	329	487	579	659	1004	1026	1064
							(b) $TmPO_4$					
295 K	133	139	186	b	304	331	488	581	662	1006	1025	1065
77 K	133	139	188	b	310	331	491	582	664	1009	1031	1070
10 K	134	137	188	b	309	330	490	580	662	1009	1031	1071

[a]Not observed at room temperature due to interfering laser plasma line.
[b]Not observed.

$$\frac{F(1,\nu)}{F(2,\nu)} = 1.3\frac{\nu}{\bar{\nu}_{\chi k}}, \tag{4}$$

where $h\bar{\nu}_{\chi k}$ is the average energy of the $(4f)^{n-1}5d$ configuration. Several lines, in both the Er^{3+} and Tm^{3+} spectra, are thus predicted to be strongly asymmetric. A study of the electronic Raman intensity pattern is then a sensitive test of the second-order theory, since only the one phenomenological parameter $F(1,\nu)/F(2,\nu)$ is required.

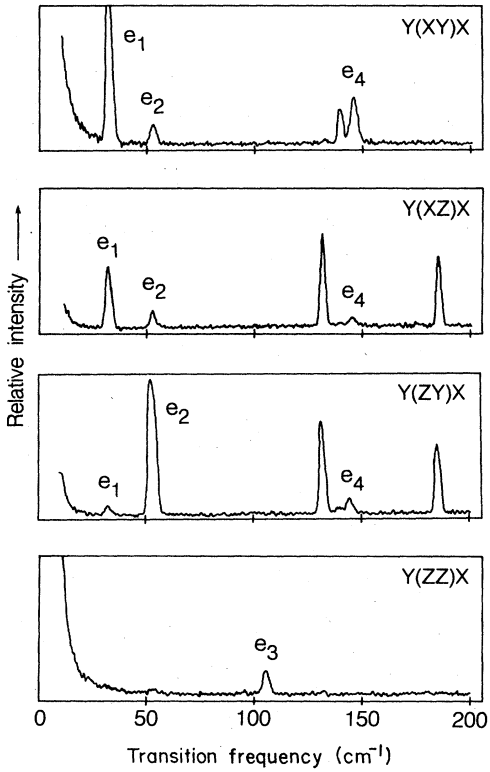

FIG. 1. 0—200-cm^{-1} Raman scans of $ErPO_4$, taken at approximately 10 K with the 514.5-nm line of the Ar^+ laser. All slits were at 200 μm. Lines e_1 through e_4 correspond to the electronic transitions at 33, 53, 105, and 145 cm^{-1}. Full scale is 600 counts/sec and the peak intensity of the 33-cm^{-1} line in XY is 1200 counts/sec. The phonon line at 140 cm^{-1} in XY is leakage from the XX polarization.

V. $ErPO_4$ EXPERIMENTAL RESULTS

The phonon frequencies and their symmetries at 295, 77, and approximately 10 K are listed in Table III. Our 295 K frequencies agree with the room-temperature values of Begun *et al.*[12] however, we differ in the symmetry assignments. Our assignments are in agreement with those given in previous studies of the phosphate crystals.[20]

Transitions from the Γ_7 ground state to excited levels in the $^4I_{15/2}$ ground manifold were studied. A total of four electronic lines were observed and have been listed in Table I. The frequencies are in good agreement with the values for Er^{3+} in $LuPO_4$. In the 200—300 cm^{-1} frequency range several broad and weak features that could not convincingly be shown to be electronic Raman transitions were observed. Only the transitions appearing in the 0—200 cm^{-1} region are discussed.

Figure 1 displays the XY-, XZ- ($=YZ$), ZY- ($=ZX$), and ZZ-polarization Raman scans of $ErPO_4$ at approximately 10 K, in the 0- to 200-cm^{-1} region, excited with the 514.5-nm line of the Ar^+ laser. The asymmetry of the scattering for the 34- and 53-cm^{-1} lines is striking. As predicted by the second-order theory, for the 34-cm^{-1} transition $I_{XZ,YZ}$ is greater than $I_{ZX,ZY}$, and for the 53-cm^{-1} transition $I_{XZ,YZ}$ is less than $I_{ZX,ZY}$. The phonon

TABLE IV. Comparison of observed and predicted asymmetry ratios $I_{XZ,YZ}/I_{ZX,ZY}$ for the electronic Raman transitions of $ErPO_4$. The maximum relative error on the observed ratios is ±50% and $F(1,\nu)/F(2,\nu)=0.25$ was used for the predicted ratios.

	Transition		
	33 cm^{-1}	53 cm^{-1}	145 cm^{-1}
Observed asymmetry	5.3	0.2	0.6
Predicted asymmetry	3.5	0.04	1.9

TABLE V. Predicted and observed intensities of the electronic Raman transitions from the ground-state to the crystal-field levels of the $^4I_{15/2}$ multiplet of $ErPO_4$. The calculated intensities are in units of $[F(2,\nu)]^2\times 10^{-4}$ and the observed intensities have been scaled so that calculated and observed intensities are equal for the ZX,ZY component of the 53-cm^{-1} transition. $F(1,\nu)/F(2,\nu)=0.25$ was used. The polarization convention is described in Ref. 25.

Transition	Polarization	Predicted intensity	Observed intensity
33 cm^{-1}	XX,YY	0.6	Not observed
	XY,YX	15.2	106.6
	XZ,YZ	46.6	20.8
	ZX,ZY	13.1	3.9
53 cm^{-1}	XX,YY	0.04	Not observed
	ZZ	0.2	Not observed
	XY,YX	14.6	6.5
	XZ,YZ	1.8	6.5
	ZX,ZY	42.9	42.9
105 cm^{-1}	XX,YY	1.7	Not observed
	ZZ	7.8	10.4
	XY,YX	1.7	Not observed
	XZ,YZ	0.6	Not observed
	ZX,ZY	0.4	Not observed
145 cm^{-1}	XX,YY	0.2	Not observed
	XY,YX	8.4	13.0
	XZ,YZ	4.9	3.9
	ZX,ZY	2.5	6.5

lines (see Table III) remain quite symmetric. It should be pointed out that resonance effects cannot be causing this asymmetry, since both the 514.5- and 457.9-nm lines are not in resonance with any higher-lying electronic states. Also, they both yield identical Raman spectra.

The asymmetry for a particular transition is measured by the ratio $I_{XZ,YZ}/I_{ZX,ZY}$, and two mathematical values can be extracted for $F(1,\nu)/F(2,\nu)$, since the intensities depend on the $|\alpha_Q^K|^2$. Discarding the unrealistic one, the 33-cm^{-1} line yields for $F(1,\nu)/F(2,\nu)$ the value 0.20 ± 0.05, while the 53-cm^{-1} line yields 0.37 ± 0.09. These are reasonably close to the predicted value of 0.25, using Eq. (4) and $\bar{\nu}_{5d}=115\,000$ cm^{-1}.[26] For the weak 145-cm^{-1} line the experimental uncertainty is such that it is not possible to obtain an accurate value for $F(1,\nu)/F(2,\nu)$. The predicted and observed asymmetries for the $ErPO_4$ transitions, as given by $I_{XZ,YZ}/I_{ZX,ZY}$, are compared in Table IV. The 105-cm^{-1} transition is not listed since it appears only in ZZ polarization.

The predicted and observed intensities of the electronic Raman transitions for different polarization combinations are shown in Table V. The calculated intensities are in units of $[F(2,\nu]^2\times10^{-4}$, and the ratio $F(1,\nu)/F(2,\nu)=0.25$ was used. Since the experimental intensities are in arbitrary units, for comparison purposes they were scaled by a constant factor such that predicted and observed intensities for the 53-cm^{-1} transition for polarization ZX,ZY were equal. This amounts to measuring the intensities relative to the 53-cm^{-1} line for ZX,ZY. The agreement between observed and calculated values is not unreasonable. The worst discrepancy is for the XY,YX component of the 33-cm^{-1} transition where there is a difference of a factor of 7 between the two values. For all the other transitions, predicted and observed intensities differ at most by factors of 2 to 4.

VI. $TmPO_4$ EXPERIMENTAL RESULTS

$TmPO_4$ has previously been the subject of an electronic Raman scattering study.[13] Our spectra agree with those shown in that work. Our phonon lines (Table III) have the same symmetry assignments as those of Guha,[13] but disagree in frequency for the higher-lying phonons. Other reported room-temperature frequencies[12] are in agreement with those of Table III.

The observed transitions were between the ground-state and the crystal-field levels of both the $^3H_6$ ground manifold and the $^3F_4$ first excited manifold. The latter represents a Raman shift in excess of 5000 cm^{-1}. The electronic levels observed via the Raman transitions are shown in Table II. The ground-multiplet energies agree with those of Guha.[13] In this work, however, the level at 84 cm^{-1} is assigned to the symmetry representation Γ_3. Note that the relative positions of several of the $TmPO_4$ $^3F_4$ levels are different from those of Tm^{3+}:$LuPO_4$.

The XZ ($=YZ$), XY, and ZY ($=ZX$) Raman scans of $TmPO_4$ in the 0—300 cm^{-1} range at approximately 10 K are shown in Fig. 2. The line at 84 cm^{-1} is one of the strongest peaks in the spectrum, its intensity being comparable to that of the 1000-cm^{-1}-region phonons.

The asymmetry features of the Γ_5 electronic lines have been studied in detail. The three lines at 30, 138, and 280 cm^{-1} are predicted to be strongly asymmetric. However, the observed and predicted patterns are quite different.

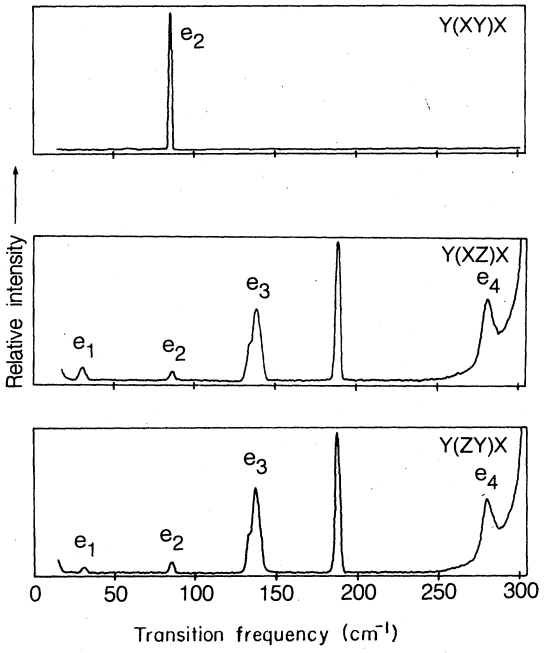

FIG. 2. 0—300 cm^{-1} Raman scans of $TmPO_4$, taken at approximately 10 K with the 514.5-nm line of the Ar^+ laser. All slits were at 200 μm. Lines e_1 through e_4 correspond to the electronic transitions at 30, 86, 138, and 280 cm^{-1}. Full scale is 25 000 counts/sec for the XY scan, and 2500 counts/sec for the other scans.

For instance for the 30-cm^{-1} line the second-order theory predicts the ratio $I_{XZ,YZ}/I_{ZX,ZY}=0.1$, whereas we find experimentally $I_{XZ,YZ}/I_{ZX,ZY}=3.0$. The observed and predicted asymmetry ratios are listed in Table VI. With

TABLE VI. Comparison of observed and predicted asymmetry ratios $I_{XZ,YZ}/I_{ZX,ZY}$ for the electronic Raman transitions of $TmPO_4$. The maximum relative error on the observed ratios is ±50%.

	Transition		
	30 cm^{-1}	138 cm^{-1}	280 cm^{-1}
Observed asymmetry	3.0	0.9	1.2
Predicted asymmetry with $F(1,\nu)/F(2,\nu)=0.25$	0.1	5.8	0.5
Predicted asymmetry with $F(1,\nu)/F(2,\nu)=-0.03$	3.1	0.8	1.1

$F(1,\nu)/F(2,\nu)=0.25$ (the average positions of the Er^{3+} and Tm^{3+} $5d$ configurations are roughly the same[26]) there is a clear conflict between theory and experiment. The asymmetry ratios have also been calculated using $F(1,\nu)/F(2,\nu)=-0.03$, an unrealistic value if one considers Eq. (4), but which yields a much better fit to the experimental data. Resonance effects cannot be playing a role as the intensities are the same for excitation with both the 514.5- and 488.0-nm lines of the Ar^+ laser.

The predicted and observed intensities for the electronic Raman transitions in $TmPO_4$ from the ground-state to the crystal-field levels of the $^3H_6$ manifold are listed in Table VII. Table VII(a) has been calculated with $F(1,\nu)/F(2,\nu)=0.25$, and Table VII(b) with $F(1,\nu)/F(2,\nu)=-0.03$. The calculated values are in units of $[F(2,\nu)]^2\times10^{-4}$. The observed values were scaled so that predicted and observed intensities for the 86-cm^{-1} transition were equal. With $F(1,\nu)/F(2,\nu)=-0.03$ there appears to be better agreement between calculated and ob-

TABLE VII. Predicted and observed intensities of the electronic Raman transitions from the ground state to the crystal-field levels of the $^3H_6$ multiplet of $TmPO_4$. The calculated intensities are in units of $[F(2,\nu)]^2\times10^{-4}$ and the observed intensities have been scaled so that calculated and observed intensities are equal for the 86-cm^{-1} transition. The polarization convention is described in Ref. 25.

Transition	Polarization	Predicted intensity	Observed intensity
	(a) $F(1,\nu)/F(2,\nu)=0.25$ used for the predicted values		
30 cm^{-1}	XZ,YZ	6.6	3.7
	ZX,ZY	43.2	1.2
86 cm^{-1}	XY,YX	228.0	228.0
138 cm^{-1}	XZ,YZ	25.8	21.6
	ZX,ZY	3.7	24.0
183 cm^{-1}	XY,YX	11.1	Not observed
248 cm^{-1}	XX,YY	10.2	Not observed
	ZZ	41.0	Not observed
254 cm^{-1}	XX,YY	47.6	Not observed
280 cm^{-1}	XZ,YZ	5.6	23.4
	ZX,ZY	11.7	20.3
303 cm^{-1}	XY,YX	0.4	Not observed

TABLE VII. (*Continued*).

Transition	Polarization	Predicted intensity	Observed intensity
321 cm^{-1}	XX, YY	7.8	Not observed
	(b) $F(1,\nu)/F(2,\nu)=-0.03$ used for the predicted values		
30 cm^{-1}	XZ, YZ	6.5	3.7
	ZX, ZY	2.1	1.2
86 cm^{-1}	XY, YX	228.0	228.0
138 cm^{-1}	XZ, YZ	11.0	21.6
	ZX, ZY	13.6	24.0
183 cm^{-1}	XY, YX	0.2	Not observed
248 cm^{-1}	XX, YY	10.2	Not observed
	ZZ	41.0	Not observed
254 cm^{-1}	XX, YY	47.6	Not observed
280 cm^{-1}	XZ, YZ	8.8	23.4
	ZX, ZY	8.0	20.3
303 cm^{-1}	XY, YX	0.4	Not observed
321 cm^{-1}	XX, YY	7.8	Not observed

served values, and the strength of the 86-cm^{-1} line relative to the other transitions is reasonably well accounted for in both cases. Several lines, in particular those at 248 and 254 cm^{-1}, are predicted to be quite strong, but are totally absent from the experimental spectra. Note that there are no close-lying phonons to mask these two lines. The intensities of the transitions from the ground state to the crystal-field levels of the $^3F_4$ manifold are listed in Table VIII. Again, the observed values were scaled with respect to the 86-cm^{-1} line. For the $^3F_4$ transitions the antisymmetric tensor does not appear so that there is no adjustable parameter for the relative intensities. It can be seen that the agreement between observed and calculated values is not unreasonable.

Thus, while the second-order theory accounts, in a very qualitative way, for the $TmPO_4$ electronic Raman intensities, it appears to be inadequate with regard to the asymmetry patterns as well as the intensities of the electronic Raman transitions from the ground state to the crystal-field levels of the $^3H_6$ multiplet. The discrepancies for $TmPO_4$ are seen to be much worse than in the case of $ErPO_4$.

TABLE VIII. Predicted and observed intensities of the electronic Raman transitions from the ground-state to the crystal-field levels of the $^3F_4$ multiplet of $TmPO_4$. The calculated intensities are in units of $[F(2,\nu)]^2\times10^{-4}$ and the observed intensities have been scaled as in Table VII. The polarization convention is described in Ref. 25.

Transition	Polarization	Predicted intensity	Observed intensity
5602 cm^{-1}	XY, YX	30.3	39.4
5676 cm^{-1}	XX, YY	10.9	Not observed
	ZZ	43.6	9.2
5688 cm^{-1}	XZ, YZ, ZX, ZY	24.0	9.9
5735 cm^{-1}	XY, YX	0.0	Not observed
5763 cm^{-1}	XY, YX	2.0	Not observed
5842 cm^{-1}	XZ, YZ, ZX, ZY	0.5	Not observed
5870 cm^{-1}	XX, YY	13.0	Not observed
	ZZ	51.8	20.9

VII. CONCLUSION

It has been shown that low-temperature electronic Raman scattering between individual crystal-field levels of rare-earth-doped crystals is a sensitive method of testing the standard second-order Judd-Ofelt—type theories of two-photon processes. The appearance of asymmetric features has been found to be particularly useful in this investigation. In the comparison between experimental and calculated intensities, the second-order theory is qualitatively correct for both $ErPO_4$ and $TmPO_4$, but a more detailed study reveals serious flaws in the $TmPO_4$ case. For $ErPO_4$ the theory works somewhat better.

It is possible that higher-order terms in the perturbation expansion, involving interactions in the higher excited states (spin-orbit, crystal field, or electrostatic) are needed to explain the discrepancies, as was the case for the two-photon absorption work.[2–5]

ACKNOWLEDGMENTS

This work was supported in part by the Director, Office of Energy Research, Office of Basic Energy Sciences, Chemical Sciences Division of the U.S. Department of Energy under Contract No. DE-AC03-76SF00098. Oak Ridge National Laboratory is operated by Martin Marietta for the U.S. Department of Energy under Contract No. W-7405-eng-26.

[1]M. Dagenais, M. Downer, R. Neumann, and N. Bloembergen, Phys. Rev. Lett. **46**, 561 (1981).

[2]B. R. Judd and D. R. Pooler, J. Phys. C **15**, 591 (1982).

[3]M. C. Downer, A. Bivas, and N. Bloembergen, Opt. Commun. **41**, 335 (1982).

[4]M. C. Downer and A. Bivas, Phys. Rev. B **28**, 3677 (1983).

[5]M. C. Downer, C. D. Cordero-Montalvo, and H. Crosswhite, Phys. Rev. B **28**, 4931 (1983).

[6]J. D. Axe, Phys. Rev. **136A**, 42 (1964).

[7]O. Mortensen and J. A. Koningstein, J. Chem. Phys. **48**, 3971 (1968).

[8]J. A. Koningstein and O. Mortensen, Phys. Rev. **168**, 75 (1968).

[9]J. A. Koningstein and O. Mortensen, J. Opt. Soc. Am. **58**, 1208 (1968).

[10]J. A. Koningstein and P. Grunberg, Can. J. Chem. **49**, 2336 (1971).

[11]J. A. Koningstein and O. Mortensen, Nature (London) **217**, 445 (1968).

[12]G. M. Begun, G. W. Beall, L. A. Boatner, and W. J. Gregor, J. Raman Spectrosc. **11**, 273 (1981).

[13]S. Guha, Phys. Rev. B **23**, 6790 (1981).

[14]T. Hayhurst, G. Shalimoff, N. Edelstein, L. A. Boatner, and M. M. Abraham, J. Chem. Phys. **74**, 5449 (1981).

[15]P. C. Becker, T. Hayhurst, G. Shalimoff, J. G. Conway, N. Edelstein, L. A. Boatner, and M. M. Abraham, J. Chem. Phys. **81**, 2872 (1984).

[16]L. A. Boatner, M. M. Abraham, and M. Rappaz, in *Scientific Basis for Nuclear Waste Management,* edited by J. G. Moore (Plenum, New York, 1981), Vol. 3, p. 181.

[17]W. O. Milligan, D. F. Mullica, G. W. Beall, and L. A. Boatner, Inorg. Chim. Acta **60**, 39 (1982).

[18]G. W. Beall, L. A. Boatner, D. F. Mullica, and W. O. Milligan, J. Inorg. Nucl. Chem. **43**, 101 (1981).

[19](a) W. O. Milligan, D. F. Mullica, G. W. Beall, and L. A. Boatner, Acta Crystallogr. Sect. C **39**, 23 (1981); (b) P. Dawson, M. M. Hargreave, and G. R. Wilkinson, J. Phys. C **4**. 240 (1970).

[20]R. J. Elliott, R. T. Harley, W. Hayes, and S. R. P. Smith, Proc. R. Soc. London Ser. A **328**, 217 (1972).

[21]J. A. Koningstein, *Introduction to the Theory of the Raman Effect* (Reidel, Dordrecht, Holland, 1972), p. 155.

[22]The correct definition of the scattering amplitude for a Raman transition from state n to state k is given by

$$(\alpha_{\rho\sigma})_{nk}=-\frac{1}{h}\sum_r\left[\frac{(M_\rho)_{nr}(M_\sigma)_{rk}}{\nu_{rk}-\nu}+\frac{[\rho\leftrightarrow\sigma]}{\nu_{rn}-\nu}\right],$$

where $(M_\rho)_{nr}$ is the matrix element of the electric dipole operator, ρ and σ denote Cartesian coordinates, and $h\nu_{rk}=E(r)-E(k)$. The overall minus sign has been omitted in Refs. 7–9, and we have included it in our definition of $F(K,\nu)$ which was previously given as Eq. (8) of Ref. 8. The minus sign can be important if higher-order terms are added to the second-order amplitude.

[23]A. R. Edmonds, *Angular Momentum in Quantum Mechanics* (Princeton University Press, Princeton, N. J., 1960).

[24]C. W. Nielson and G. F. Koster, *Spectroscopic Coefficients for the p^n,d^n, and f^n Configurations* (MIT, Cambridge, Mass., 1963).

[25]In our expression for the scattering amplitude, given in Ref. 22, the incident photon's electric field vector is written to the right of that for the scattered photon. As a result in our notation we describe the direction of propagation and polarization of the photons in the following order: direction of propagation of the scattered photon (polarization of the scattered photon, polarization of the incident photon), direction of propagation of the incident photon (see Figs. 1 and 2). This is the reverse of the more commonly used Porto notation.

[26]G. H. Dieke and H. M. Crosswhite, Appl. Opt. **2**, 675 (1963).